Research Article

Hydrochars produced by hydrothermal carbonisation of seaweed, coconut shell and oak: effect of processing temperature on physicochemical adsorbent characteristics

Eric Danso-Boateng[1] · Andrew B. Ross[1] · Ted Mariner[1] · James Hammerton[1] · Melissa Fitzsimmons[1]

Abstract

The present study addresses the production of hydrochars from brown seaweed (*Fucus serratus*) (FS-HCs), coconut shell (CS-HCs), and oak (Oak-HCs) as potential adsorbents using hydrothermal carbonisation (HTC). The effect of HTC processing temperature on the physicochemical adsorbent characteristics of the hydrochars is investigated at different temperatures (200, 220, 250 °C) using a hydrothermal batch reactor. Increasing HTC temperature causes the formation of many spheres in CS-HCs and Oak-HCs, increasing their porosity, except FS-HCs. The surface area of the hydrochars increases with increasing HTC temperature; 10.93–12.78 m^2/g for FS-HCs, 2.18–21.94 m^2/g for CS-HCs, except for Oak-HCs which decreases from 4.89 to 3.09 m^2/g. Increasing HTC temperature decreases volatile matter content in the hydrochars, increases fixed carbon content, and decreases H/C ratio (except for FS-HCs) and O/C ratio of the hydrochars. For all the hydrochars, increasing the HTC temperature results in a slight decrease in zeta potential magnitude, with negatively charged surfaces, making them potential adsorbents for cationic pollutants. The study confirms that the HTC process improves key chemical and physical characteristics of the hydrochars compared to the original biomass, and that the physicochemical adsorbent characteristics are enhanced as the processing temperature increases.

Article highlights

• Hydrochars produced by hydrothermal carbonisation of seaweed, coconut shell and oak have improved physicochemical adsorbent characteristics.
• Increasing temperature results in a decrease in O/C ratio in the hydrochars, indicating a decrease in oxygenated functional groups.

• Physicochemical adsorbent characteristics of the hydrochars are influenced by the type of biomass feedstock and the processing temperature utilised.

✉ Eric Danso-Boateng, e.danso-boateng@leeds.ac.uk | [1]School of Chemical and Process Engineering, University of Leeds, Leeds LS2 9JT, UK.

1 Introduction

Adsorption technology has shown to be a promising approach for the removal of inorganic and organic contaminants from aqueous media due to its safety, simplicity and ease of operation, high availability, and high efficiency [1–4]. Activated carbon is the most commonly used adsorbents for removing pollutants from wastewaters [5]. However, the associated high costs in relation to the extremely high processing temperatures (up to 1000 °C) and low conversion efficiency to produce the activated carbon inhibit its exploration [6, 7]. Hence, because charring generally eliminates the release of secondary pollutants into the wastewater stream [8], a number of low-cost alternatives have been investigated, including the production of biochar, which is the solids product of slow pyrolysis [9, 10]. However, like activated carbons, the process requires very high temperatures (> 500 °C) and the solids yield is low (about 35%) [11], although the yields are higher than those obtained from the production of activated carbons. Therefore, the focus in recent times has been to use inexpensive and more efficient processes that can produce higher carbonised solids yields in an environmentally friendly and sustainable manner.

Currently, "hydrochar", the solids product of hydrothermal carbonisation (HTC) process has gained interest for use as an adsorbent. Hydrochars are similar to but less stable than biochars and thermally activated carbons before the activation stage. HTC requires heating of the biomass submerged in water to 180–250 °C under pressure for several minutes to several hours, reducing both the hydrogen and oxygen content of the biomass through a series of complex reactions such as hydrolysis, dehydration, decarboxylation, aromatisation, and polymerisation [12–14]. Hydrochars derived from lignocellulosic biomass such as pine needles, pine cones, and oak leaves treated at 200 °C for 12 h have been reported to have highly hydrophilic spheres at their surfaces making them water dispersible and desirable for ion binding, and hence, have the potential for use as adsorbents [15]. Román et al. [16] produced hydrochars from pistachio shells using HTC at 220 °C for 20 h and found the formation and abundance of oxygenated functional groups including hydroxyl (O-H) and carbonyl (C=O). In a recent study, the adsorption potential of hydrochars produced at 200 °C for 20 h and derived from different biomass feedstocks including egg shell, lemon peel, rice husk, coconut peat and coconut shell were investigated, which identified O–H and carboxyl (COOH) as the major functional groups and varying surfaces areas [17]. It is evidence from these studies that the type of the biomass material influences the surface structure and functionality of the produced hydrochar. Activation has been found to influence the adsorption properties of hydrochars. For instance, HTC of cow manure was investigated at 190 and 230 °C, with or without pyrolysis post-treatment as potential adsorbent materials, and revealed that the pyrolysing the hydrochars at 600 °C for 30 min significantly increased the surface area of the hydrochars, but their adsorption capacity was three times lower than the non-pyrolysed ones [18]. However, methylene blue adsorption using NaOH-activated coconut shell derived hydrochar produced at 200 °C for a residence time of 2 h showed that NaOH-activation can improve the BET surface area and adsorption capacity of the produced hydrochars [19]. The addition of surfactant, sodium dodecylbenzenesulfonate, has been found to increase the surface area of hydrochar derived from coconut shell at an HTC temperature of 210 °C for 30 min residence time [20]. However, most of these studies did not investigate some of the essential parameters that could help to better understand characteristics of the adsorbents such as the elemental (CHNO) compositions, proximate analysis, and zeta potential of the hydrochars. Besides feedstock characteristics, HTC process conditions also influence the properties of hydrochars, which need further investigations. A study by Elaigwu and Greenway [21] conducted microwave-assisted HTC of coconut shell at different HTC process conditions by varying the reaction temperature from 150 to 200 °C and residence time from 5 to 30 min. Their study revealed that HTC led to changes in the chemical and structural compositions as well as improved the energy properties of the produced hydrochars. However, while conventional HTC is known to improve the BET surface area of hydrochars [17, 19], the formation of tarry substances during the microwave-assisted HTC contaminated the hydrochar by blocking the pores, resulting in a small BET surface area [21]. A recent study on the adsorption capacity of orange peel and grape skin derived hydrochars produced at HTC temperatures between 180 and 250 °C have shown that hydrochars produced at lower temperature (180 °C) have low surface area, but adsorption of methylene blue is the highest, because of their maximum density of total oxygen functional groups, which decrease with the increase in HTC temperature [22]. The findings from these studies revealed that HTC process conditions and the initial composition and structure of the biomass material can greatly influence the shape, size, surface structure, and adsorption characteristics of the final hydrochar. Hence, a full investigation of the physicochemical adsorbent characteristics of hydrochars derived from a variety of biomass feedstock at different HTC temperatures is required.

The development of practical and efficient adsorbents from readily available and low-cost materials is desirable. In this present work, brown seaweed (*Fucus serratus*), coconut shell and oak sawdust were carbonised to produce hydrochars to study their physicochemical sorption characteristics. Seaweed is a widely available macroalgae found on the shores of the North Atlantic Ocean [23] and can be cultivated on many coastlines; hence it does not compete for land with food crops. About 62 million metric tons of coconut waste is produced annually [24], of which the shell represents approximately 18 million tonnes [25]. Sawdust, including oak derived types are wastes generated from sawmills and the furniture industry, which makes it a readily available biomass source. Converting these biomass wastes to hydrochars for use as adsorbents, especially oak sawdust and coconut shell, would prevent biodegradation of the biomass that could have caused the emission of greenhouse gases and that is, contribute to global warming.

Although the composition of seaweeds is complex compared with lignocellulosic biomass, studies into the sorption potential of non-carbonised seaweeds for pollutant removal has gain research interest in recent times, and have shown to have distinct sorption characteristics [26, 27]. However, studies into the sorption characteristics of seaweed-derived hydrochars are limited in the literature, and further studies are required to fully understand the impact of carbonisation on their physicochemical sorption characteristics in comparison to their raw biomass feedstocks. Coconut shell and oak are lignocellulosic biomass, but their compositions vary depending on the species. Hence, it is important to understand the physicochemical sorption characteristics of hydrochars derived from both feedstocks. Coconut shell contains 15–27% of cellulose, 41–45% of lignin, and 18–40% of hemicellulose [19, 28, 29]. Oak wood is mainly composed of cellulose (38–46%), hemicellulose (19–30%) and lignin (22–29%), while French oak comprises of cellulose (22–50%), hemicellulose (17–30%) and lignin (17–30%) [30]. Although studies on the adsorption properties and physicochemical sorption characteristics of hydrochars derived from coconut shell and oak are available in the literature, most of the physicochemical sorption characteristics have not been fully reported; therefore, further investigations are required in these areas.

The aim of this study was to investigate the hydrochar properties relevant to its potential physicochemical adsorbent characteristics from a range of feedstocks including brown seaweed (*F. serratus*), coconut shell and oak wood sawdust. In addition to the fact that information on the physicochemical sorption characteristics of coconut shell and oak hydrochars have not been fully reported, both biomass materials being mainly lignocellulosic were included for comparison with seaweed, which has a rather complex composition. The hydrochars were characterised using elemental analysis, proximate analysis, Fourier transform infrared (FTIR), scanning electron microscopy (SEM), Brunauer–Emmett–Teller (BET) surface area, and zeta potential. The effect of HTC temperature on the physicochemical adsorbent characteristics has been investigated to increase the understanding of the best conditions to produced hydrochars with improved functionality.

In the next section, we describe the raw materials used and experimental and characterisation methods. Section 3 presents the results and the discussion the interpretation of the experimental results. In Sect. 4, we present a conclusion of the experimental findings.

2 Materials and methods

2.1 Raw materials

The *F. serratus* was collected by hand near Aberystwyth, UK (52° 25′ 11″ N, 4° 05′ 16″ W) in July 2019. Samples were initially frozen and then subsequently freeze dried. The coconut shell was obtained by de-shelling whole coconut purchased at the local supermarket in Leeds, UK. After the coconut water and flesh were removed, the shells were broken into small pieces with a hammer. The oak wood was collected from Holm Oak trees, debarked and chipped into pieces of about 1.0 cm. The two lignocellulosic biomass samples were air-dried at room temperature in a fume cupboard for 2 days to remove the moisture to aid milling. Each dried biomass was separately milled with a Retsch Cutting Mill SM300 at 1500 RPM to reduce the particle size to between 0.1 and 1.0 mm, and then separately stored in sealed containers to prevent contamination.

2.2 Production of hydrochars

HTC was conducted in a 2-l batch autoclave (Parr USA) in quartz glass inserts. A biomass-to-water ratio of about 1:4 (w/v) was used to obtain a solid loading of approximately 20%. Higher solid loading greater than 15% lead greater extent of carbonisation [37]. The mixture was mixed completely to submerge the biomass, and then heated at three different temperatures of 200 °C, 220 °C and 250 °C for a residence time of 2 h. The temperature fluctuation on the HTC reactor was ±5°C. After a completion of each run, the reactor was allowed to cool to room temperature, and the vapour phase was vented in a fume cupboard. The mixture was filtered using a Whatman filter paper Grade 1 (with 11 μm pores) and a Büchner funnel to separate the hydrochar from the liquid by-product. During filtration, the hydrochar was washed with deionised waster to remove

any remaining process water. The hydrochar was then allowed to dry at room temperature for 2 days to remove any residual moisture and then weighed to determine the mass of the hydrochar. The HTC process was repeated for each biomass feedstock at each reaction temperature. The hydrochars were classified according to the HTC temperature as follows: FS-HC200, FS-HC220, and FS-HC250 for the *F. serratus* hydrochars (FS-HC); CS-HC200, CS-HC220, and CS-HC250 for the coconut shell hydrochars (CS-HC); and Oak-HC200, Oak-HC220, and Oak-HC250 for the oak hydrochars (Oak-HC). The hydrochar mass yield was calculated according to Eq. (1):

$$\text{Solid yield}(\%) = \frac{\text{Mass of solids remaining after drying}}{\text{Mass of biomass feedstock}} \times 100$$

(1)

Liquid yield was calculated by difference between mass of initial water and the filtrate plus the water lost in the char during drying. Gas yield was estimated by subtracting the sum of hydrochar yield and liquid yield from 100.

2.3 Characterisation of the hydrochars

Elemental carbon, hydrogen, and nitrogen (CHN) in the raw biomass and the hydrochars were determined using a Flash EA112 Elemental Analyser (Thermo Scientific, Rodana, Italy) in line with ASTM D5373-08 [31]. Residual moisture, volatile matter, and ash were measured using a thermogravimetric analyser (TGA-Q5000, TA Instruments, UK) according to ASTM method D7582-10 [32].

FTIR spectra were obtained at a wavelength from 4000 to 400 cm^{-1} using an FTIR spectrometer (Spotlight 400 N FT-NIR, PerkinElmer, UK) to analyse organic functional groups of the hydrochars.

Zeta potential of the hydrochars was analysed using a zeta potential analyser (Zetasizer Nano ZS, Malvern, UK). To perform the analyses, the milled samples were suspended in water at a concentration of 0.5% (wt). An extract of the

suspension was injected into the capillary cell and inserted in the Zetasizer and analysed for the zeta potential. The method was repeated for all the remaining samples.

The surface morphology of the raw biomass and the hydrochars was analysed using a Hitachi TM3030Plus SEM. The sample holder was covered in conductive graphite tape with adhesive sides after which a small amount of the sample was carefully and evenly placed onto the graphite tape avoiding large piles. The sample holder was placed into the chamber of the microscope and the air within was removed with a vacuum pump. Images were taken using secondary electrons produced by a 15 kV electron beam at magnifications of ×100, ×500, ×2000, and ×5000.

The surface area and pore volume of all the hydrochars were measured from nitrogen isotherms using a surface area analyser (Quantachrome NOVA 2200, Quantachrome Instruments, US).

3 Results and discussion

3.1 HTC tests

The solid, liquid and gas yields of the HTC tests were calculated for each biomass from the weights that were recorded after the experiments. Table 1 reports the yield of the hydrochar, the liquid by-products, and gas at the different HTC process temperatures (200, 220, and 250 °C).

As shown in Table 1, the oak produced the highest solids followed by the coconut shell and then the *F. serratus*. This may be caused by the variation in the composition of the three biomass feedstocks. Coconut shell and oak are lignocellulosic biomass comprising of lignin, hemicellulose and cellulose [19, 28, 29]. The higher yield of Oak-HCs means that the oak used has a high lignin content, which decomposes at higher temperatures [33]. Lignin has a more stable phenolic structure, which requires higher processing temperature above the range of temperature used

Table 1 Solid, liquid and gas yield after HTC experiments

Feedstock	HTC temperature (°C)	Solid yield (%)	Liquid yield (%)	Gas yield (%)
Fucus serratus	200	39.58	50.35	10.07
Fucus serratus	220	41.11	45.49	13.41
Fucus serratus	250	38.65	47.42	13.92
Coconut shell	200	64.57	30.61	4.82
Coconut shell	220	63.30	29.05	7.65
Coconut shell	250	55.59	31.83	12.58
Oak wood	200	71.79	21.55	6.66
Oak wood	220	71.20	19.41	9.38
Oak wood	250	78.09	9.66	12.25

Gas yield = 100 − (hydrochar yield + liquid yield)

in this study to breakdown [33, 34]. Feedstock with higher percentage of lignin is found to produce higher solid yields [35, 36]. Coconut shell produced intermediate solid yields, which means its cellulose fraction was only partially broken down at the processing temperatures below 220 °C due to its crystalline structure, and when the temperature was increased to 250 °C the yield significantly reduced as the lignin component started to decompose. The results of coconut shell solid yields are supported by the findings of Volpe et al. [36]. In their study cellulose decomposed above 220 °C, with a significant decreased in hydrochar yield of 53.4% obtained at 230 °C compared with 82.4% at 220 °C, and a more thermally stable solid product was formed between 240 and 280 °C.

With increasing temperatures above 220 °C, that is increasing the reaction severity, there was a reduction in solid yield as the cellulose began to decompose and more material was converted into gas [14, 22, 36]. This explains the increased in gas yield when there was a rise in the HTC processing temperatures. The decreased in solid yield at higher temperatures was also caused by loss of the feedstock to the liquid products due to the increased rates and extent of reaction [6, 37], resulting in an increase in the liquid yield.

Oak and *F. serratus* did not follow the trend of decreasing solid yield with rising HTC temperature. Oak solid yield increased at 250 °C, which may be due to polymerisation reactions leading to the continued reaction of the lignin intermediates to secondary hydrochar [38], as well as extensive condensation/intermolecular dehydration and formation of polymers (polymerised product) [39]. Sevilla and Fuertes [40] reported a small increase in hydrochar yield produced from cellulose when the temperature was increased from 230 to 250 °C. Zhu et al. [41] found similar results, in which a porous carbon with relatively high hydrochar yield was derived from *Salix psammophila* at a high HTC peak temperature and retention time and explained that more stable hydrochar appears to resist chemical activation. Unlike coconut shell and oak which are lignocellulosic, *F. serratus* has a rather different and complex composition and contains different carbohydrates including laminarin, alginates, mannitol and sulphated fucoidan. *Fucus serratus* also contains high levels of polyphenols and higher protein content and ash content [42, 43]. It is clear that there was significant decomposition of the carbohydrates at 200 °C, which resulted in more transfer of the decomposed materials to the liquid phase. As the HTC temperature was increased to 220 °C, there was an increase in solid yield with a reduction in liquid yield, which may be caused by polymerisation reactions and recombination of the materials to char [38, 39]. As the temperature was further increased to 250 °C,

the materials decomposed, resulting in a slight decrease in the solid yield.

In comparison, due to the extremely higher temperatures used in pyrolysis, solid yields of biochar are much lower than hydrochar, as low as 20–30% for similar biomass feedstocks [44]. Including an additional activation step to produce activated carbons, reduces the solid yields further to 15–20% [45, 46]. This means hydrochars are potentially a much better option for producing carbonised solids. However, evaluation of the other characteristics of the hydrochars and adsorption analyses of the materials are required in order to choose hydrochars as better adsorbents over biochars or activated carbons.

3.2 Surface structure

SEM images showing the surface structure of the prepared hydrochar and their corresponding raw biomass are presented in Figs. 1, 2 and 3. The SEM images did not show very noticeable differences between the raw *F. serratus* and its hydrochars. However, a close comparison between the raw sample (Fig. 1a) to the hydrochars shows that some solid-to-solid conversion can be observed at magnification ×500 (Fig. 1b–d), which do not show the presence of microspheres. This suggests that microspheres were not produced in this biomass. This is due to the low concentration of cellulose in *F. serratus* resulting in a lack of intermediary molecules for polymerisation. Figure 1b–d show many nanometres (nm) sized particles, which were absent in the raw *F. serratus* and are probably similar in composition to the microspheres.

Figure 1b–d show that there is some change in the surface structure of the FS-HCs when increasing HTC temperature, though there seems to be a little change, making it difficult to notice a clear trend. Figure 1e shows some deposits on the raw *F. serratus*, which may be KCl and NaCl salts because the sample was collected from the ocean [47]. The salts will cause secondary pollution modifying the treated water if raw *F. serratus* is used as adsorbent for wastewater treatment [48]. Also, the Na Alginate and mannitol would also dissolve [42, 49]. The hydrochar shows one of the few collections of microspheres, which is probably due to carbonisation of the alginate (Fig. 1f).

Figure 2 shows the SEM images of the raw coconut shell and its hydrochars. The hydrochar produced at 200 °C (CS-HC200) (Fig. 2a) indicates that solid-to-solid conversion started to form on some parts of the sample while some microspheres begin to form. Only a small fraction of the microspheres were present at this temperature as cellulose, which starts to decompose at temperatures above 220 °C. In Fig. 2c, the hydrochar produced at 220 °C (CS-HC220) shows the formation of pores within the structure. These pores within CS-HC220
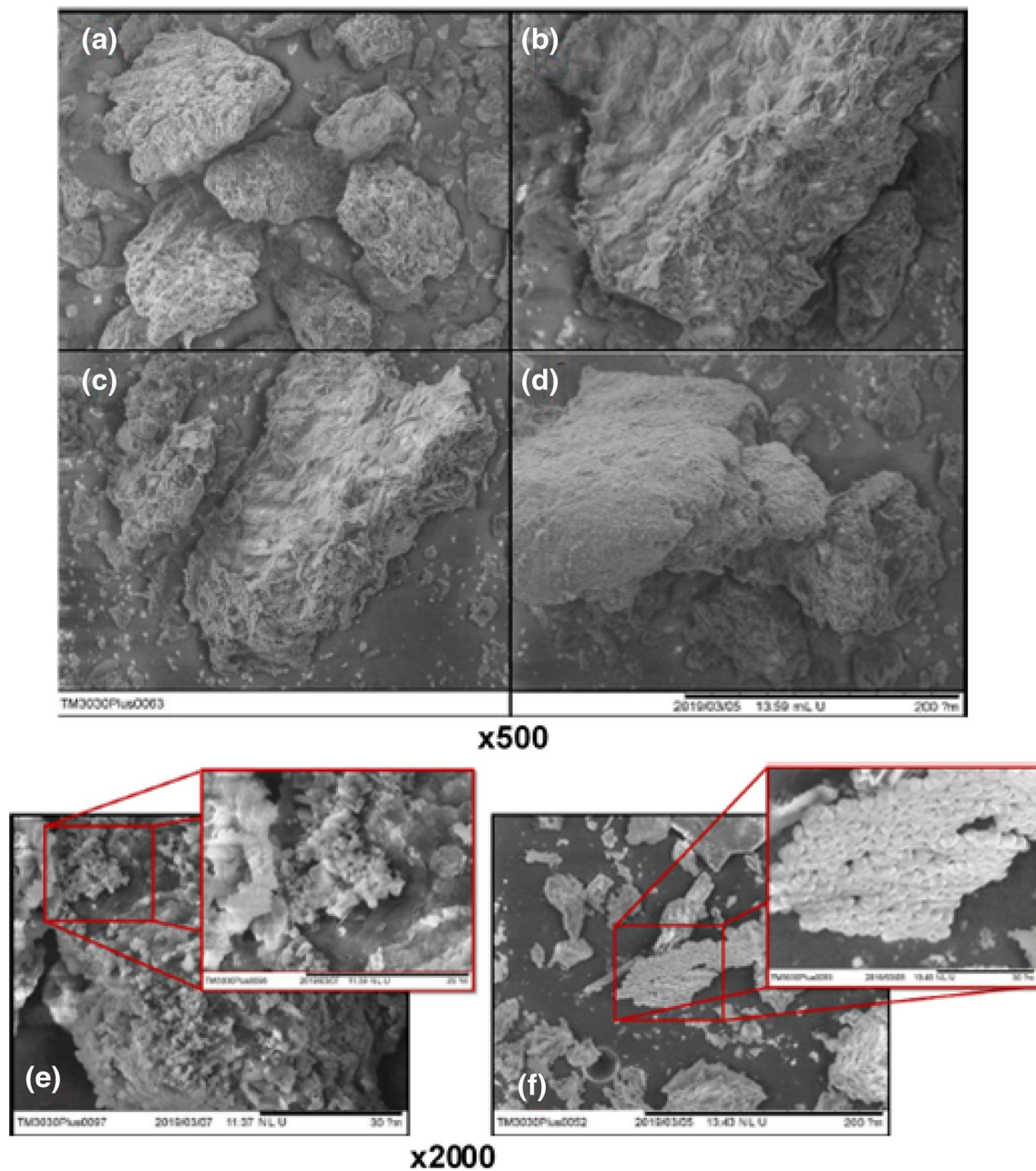
Fig. 1 SEM images at ×500 magnification of **a** raw *F. serratus*, **b** FS-HC200, **c** FS-HC220, and **d** FS-HC250. At ×2000 magnification are images of **e** deposits on raw *F. serratus*, and **f** small cluster of microspheres formed with FS-HC250

suggests that solid-to-solid conversion occurred simultaneously.

In Fig. 2d, the increase in temperature to 250 °C causes further polymerisation of the coconut shell. This resulted in increasing formation of pores in the CS-HC sample as the HTC temperature was increased. The presence of pores were an indication of solid-to-solid conversion; however, polymerisation of the microspheres was found to be the dominant mechanism for CS-HC formation.

Figure 2e and f show more magnified images of the CS-H220 and CS-H250 hydrochars, which shows about 2 nm pores in Fig. 2f, which suggest that increasing HTC temperature leads to increasing pores formation in the CS-HCs. This supports the pore volume results in Sect. 3.3.

The SEM structure of raw oak biomass is shown in Fig. 3a. HTC temperature at 200 °C was insufficient to hydrolyse the lignin content; hence, in Oak-HC200 the structure of the original biomass is largely maintained. However, carbon-rich materials are formed onto this
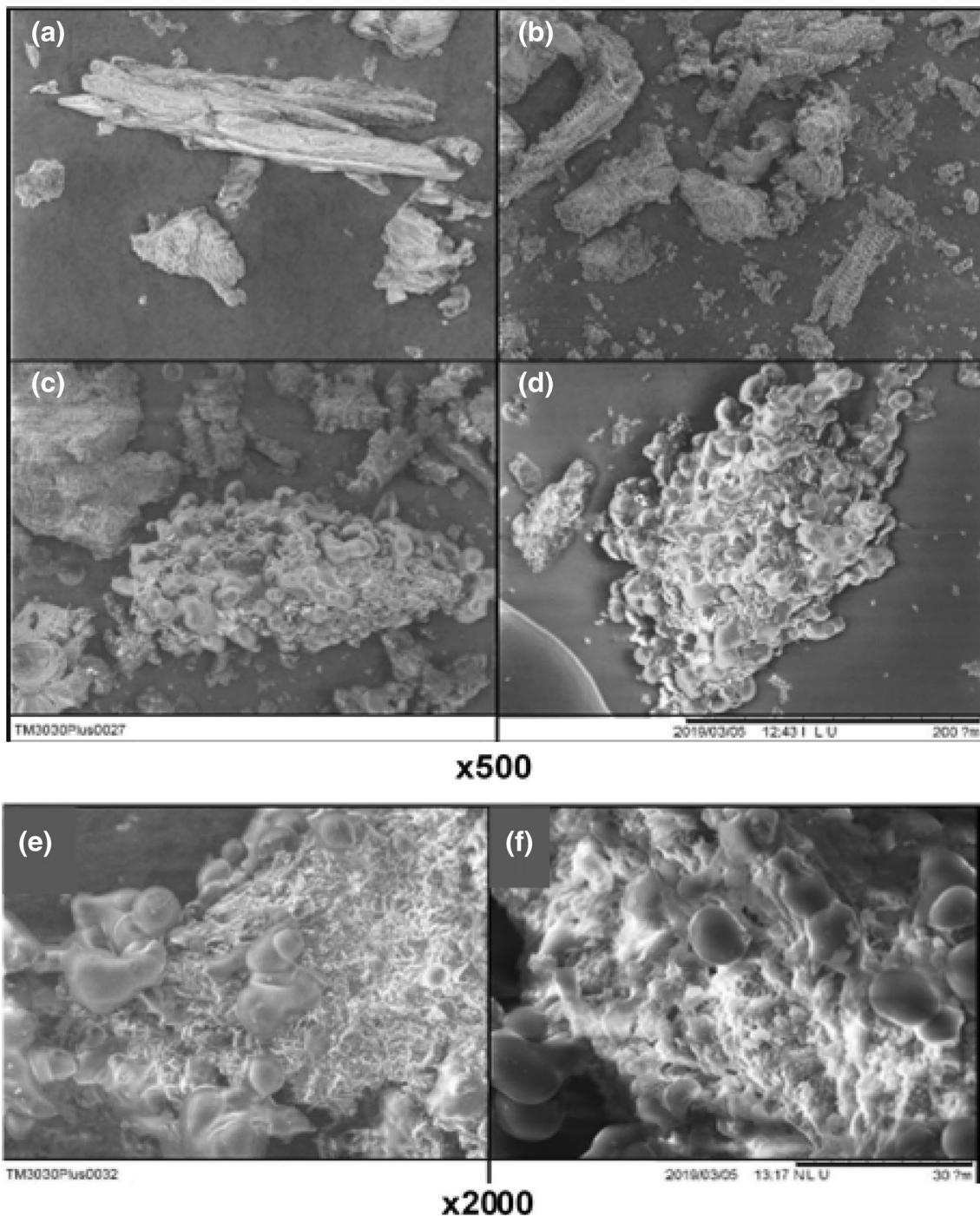
Fig. 2 SEM images at ×500 magnification of **a** raw coconut shell, **b** CS-HC200, **c** CS-HC220, and **d** CS-HC250. At ×2000 magnification are images of **e** microsphere formation on the surface of CS-H220, and **f** microsphere and pore formation on the surface of CS-HC250

skeleton in the form of small spheres (shown in Fig. 3b). This microsphere formation is clearly seen in Fig. 3c as the HTC temperature was increased to 220 °C. It has previously been reported that these microspheres are formed via the polymerisation of 5-hydroxymethylfurfural (HMF) within the aqueous phase, formed following hydrolysis

of cellulose during HTC [15]. The microspheres nucleate from the liquid intermediates onto the lignin skeleton, which undergoes minimal degradation during the HTC process and grow into carbon-rich spheres with a hydrophilic surface [35]. The hydrophilicity of the spheres makes them very easy to disperse within water when used as
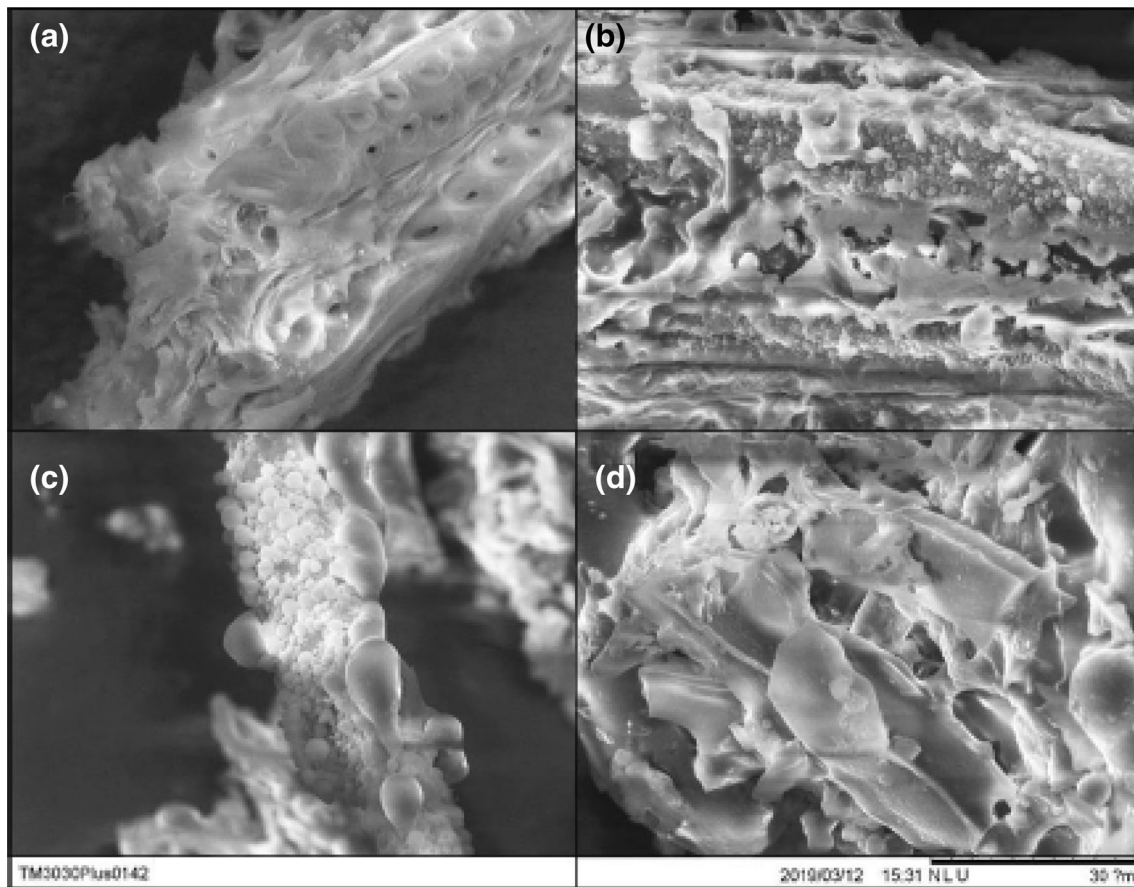
Fig. 3 SEM images at ×2000 magnification of **a** raw oak, **b** Oak-HC200 structure breakdown and microsphere formation, **c** Oak-HC220 microsphere formation, and **d** Oak-HC250 porous structure

adsorbents [15]. Figure 3d indicates that the hydrochar produced from HTC at 250 °C (Oak-HC250) shows a high abundance of microspheres, rather than a structure that is broken down, which may become less porous, and hence, might have a comparatively reduced surface area. This according to Kang et al. [35], this is due to a solid-solid heterogenous carbonisation of the non-dissolved components to form a polyaromatic char.

3.3 Surface area and pore volume

The surface area and pore volume of the hydrochars are presented in Table 2. All the raw biomass samples have low surface area and were found to be non-porous based on their surface area measurements. Hence, the data on pore volume and radius were not calculated for the raw biomass. After HTC, the surface area of the hydrochar increased with reaction severity, with the exception of Oak-HCs. Higher surface area than those obtained in this study has been reported for hydrochars derived from hazelnut shell (45.00 m²/g) carbonised at 180 °C for 4 h

Table 2 Surface area, pore volume and zeta potential of hydrochars

Material	Surface area (m²/g)	Pore volume (cm³/g)	Zeta potential (mV)
Raw FS	0.48	–	− 35.25
FS-HC200	ND	ND	− 29.90
FS-HC220	10.93	0.05	− 29.78
FS-HC250	12.78	0.04	− 27.22
Raw CS	1.12	–	− 37.35
CS-HC200	2.81	0.01	− 31.45
CS-HC220	9.63	0.02	− 29.42
CS-HC250	21.94	0.03	− 31.08
Raw Oak	0.78	–	− 23.67
Oak-HC200	ND	ND	− 28.22
Oak-HC220	4.89	0.03	− 26.63
Oak-HC250	3.31	0.01	− 24.52

ND not determined, *Raw FS* non-carbonised *Fucus serratus*, *Raw CS* non-carbonised coconut shell, *Raw Oak* non-carbonised oak

[50], walnut shell (31.00 m²/g) and sunflower stem (27.00

m^2/g) carbonised at 220 °C for 20 h [51]. The higher surface areas obtained at comparatively lower HTC temperatures may be due to the differences in the lignocellulosic compositions of hazelnut and walnut as compared to the lignocellulosic compositions of the feedstock used in this study, particularly the coconut shell and oak as explained in Sect. 3.1. Hazelnut shell contains high fraction of hemicellulose (28.20% wt.) than cellulose (24.20% wt.) and high lignin content of 34.64% (wt.) [52]. Hemicellulose decomposes at lower temperatures than cellulose and lignin [33, 34] resulting in higher surface area compared with the CS-HCs and Oak-HCs, which were mainly cellulose and lignin, respectively (as explained in Sect. 3.1). Walnut shell similarly contains hemicellulose (24.90% wt.), cellulose (30.40% wt.) and lignin (35.00% wt.) [53], whilst sunflower stalk comprises of 34–42% (wt.) cellulose, 19–33% (wt.) hemicellulose, and 12–30% (wt.) lignin [54]. Hence, the high hemicellulose and cellulose fractions will decompose at the HTC temperature of 220 °C, resulting in hydrochars of high surface areas, compared to the high cellulose- and lignin-rich CS-HCs and Oak-HCs. As explained in Sect. 3.1, FS has a different composition than lignocellulosic biomass; so, it would be difficult to make a direct comparison. Islam et al. [19] reported surface area of 876.14 m^2/g for NaOH-activated coconut shell hydrochar carbonised at 200 °C for 2 h. Tu et al. [20] found that addition of the surfactant, sodium dodecylbenzenesulfonate, during HTC of coconut shell at 210 °C for 2 h increase the surface area of hydrochar from 4.93 to 41.43 m^2/g. Although the hydrochars in this present work were not chemically activated, a comparison with these studies is useful to understand the influence of different chemical activations on the surface area of coconut shell. The surface area of CS- HC200, Oak-HC200 and Oak-HC250 are much lower, but are higher than the value of 1.30 m^2/g obtained for peanut hull hydrochar carbonised at 300 °C for 5 h [55], and within the range of values obtained for coconut peat hydrochar (2.14 m^2/g) carbonised at 200 °C for 20 h [17], and eucalyptus (4.40 m^2/g) carbonised at 250 °C for 2 h [56]. The low surface area of peanut hull is surprising, as it is highly cellulosic, containing cellulose (40.5% wt.), lignin (26.4% wt.), and hemicelluloses (14.7% wt.) [57], which should have decomposed at the HTC temperature of 300 °C applied. The surface area of CS-HC250 is similar to the value of 21.82 m^2/g obtained for a coconut shell hydrochar in a previous study conducted at the same 200 °C HTC temperature but at an extremely 20 h residence time [17], 21.00 m^2/g for pinewood hydrochar carbonised at 300 °C for 20 min [51], and olive stone hydrochar (22.00 m^2/g) carbonised at 220 °C for residence time of 20 h [58], whiles those for CS-HC220, FS-HC220 and FS-HC250 are within the range of values (8.30–15.74 m^2/g) reported for barley straw carbonised at 250 °C for 2 h [56], and rice husk hydrochar carbonised at 200 °C for 20 h

residence time [17]. These may be due to the similarities in their lignocellulosic compositions. Like coconut shell (see Sect. 3.1), olive stone, barley straw and rice husk contain high fractions of cellulose. Olive stone comprises of cellulose (31.90% wt.) than hemicellulose (21.90% wt.) and lignin (26.50% wt.) [59], whiles barley straw contains cellulose (37.60% wt.), hemicellulose (34.90% wt.) and lignin (15.80% wt.) [60], and rice husk includes cellulose (33.00% wt.), hemicellulose (26.00% wt.) and lignin (7.00% wt.) [61]. The cellulose should decompose above 220 °C [36]; hence, the similar surface areas of the olive stone and rice husk hydrochars may be attributed to the severe residence time of 20 h applied, compared to 2 h for CS-HC250 (at 250 °C) and CS-HC220 (at 220 °C). For the barley straw, the surface area may be due to the HTC temperature of 220 °C applied, which is similar to that applied in this study for CS-HC220.

Goldfarb et al. [18] reported that pyrolysed hydrochars derived from cow manure showed a surface area three orders of magnitude higher (157.70–236.50 m^2/g) than the corresponding untreated hydrochars (11.40–22.60 m^2/g), but their adsorption capacity was significantly lower. The best adsorption capacity was found for the hydrochar produced at lower HTC reaction temperature (190 °C) showing the lowest surface area and porosity, thus apparently in contrast to what is generally reported by other studies. Hence, the increased in adsorption capacity was related to the higher degree of functional groups at the surface of the hydrochar produced at the lower HTC temperature, even though the hydrochar was found to have low surface area and porosity. Similar results were found in this study. With the exception of FS-HCs, which did show any significance variation in the surface functional groups with changes in the HTC temperature, CS-HCs and Oak-HCs contain abundant surface functional groups at lower HTC temperature of 200 °C (see Sects. 3.5 and 3.7 for a detailed discussion).

Oak-HCs showed a decrease in pore volume as the HTC temperature was increased while that of the CS-HCs increased. The reduction in pore volume of the hydrochars with rising HTC temperature could be caused by the increased formation of microspheres within the pores at higher temperatures, which reduced the porosity rather than forming more surface area. It has been reported that hydrochar microspheres exhibit very low porosity [62] as the microspheres (polymerised hydrochar) are secondary hydrochar from polymerisation of monomers and dissolved fragment/polymers in the aqueous phase [40, 63]. For the CS-HCs, due to the large density of microspheres seen in the SEM images, new spheres formed on the surface of old ones while the pores increased slightly.

The pores of the Oak-HCs were about 3 nm in diameter while the other hydrochars had pores that were only 1.5 nm in diameter. Both sizes make the pores at the upper

end of the microporous or lower end of mesoporous. The smaller range of pore volumes suggests that most of the surface area of the adsorbents does not come from the pores.

3.4 Zeta potential

As shown in Table 2, the HTC process resulted in a decrease in the magnitude of the zeta potential for the *F. serratus* and coconut shell, while that of the oak increased. However, for all the hydrochars, increasing temperature resulted in a decrease in zeta potential magnitude, although not very large. The negative values indicate that the hydrochars have negatively charged surfaces making them suitable adsorbents for cationic pollutants. Particles with zeta potentials more positive than + 30 mV or more negative than − 30 mV form stable suspensions [64] as a high zeta potential is required in order to stabilise suspended particles in water due to mutual repulsion [65, 66]. The raw *F. serratus* and coconut shell have zeta potentials above the − 30 mV flocculation limit; hence, their suspensions will be stable and without the occurrence of flocculation. However, although stable solutions are good for the short term to provide good contact with the solution, high capital costs are required to remove the hydrochars from the water.

CS-HC200 and CS-HC250 have zeta potentials slightly above the − 30 mV flocculation limit; so, their suspensions will be a little stable and will not likely flocculate, whereas all the other hydrochars will flocculate in solution. The zeta potential values therefore mean that, probably except CS-HC200 and CS-HC250, flocculation can be

utilised for natural separation of the hydrochars from the aqueous solution, which is preferable. This is because the electrostatic interactions between the hydrochar particles will be reduced allowing the particles to come together and flocculate [64, 65]. Zeta potential values for hydrochar derived from sewage sludge at 210 °C and residence time of 5 h have been reported to be − 15 mV, which was increased to − 13 mV following KOH activation [67]. Zeta potential of glucose-derived hydrochar carbonised at 195 °C for a residence time of 2 h ranges between − 48.90 and − 2.67 mV over a pH range of 0.2–8.28 [68]. Although these findings are useful, the influence of HTC temperature on zeta potential of the hydrochars was not studied, and zeta potential values of biomass feedstock used in the present work have not been reported.

3.5 Elemental composition

As shown in Table 3, the carbon content of the raw biomass improved following HTC. During HTC, reactions such as hydrolysis, dehydration, decarboxylation and aromatisation occur in parallel [12, 14], removing hydrogen and oxygen to produce a carbon-rich hydrochar. For *F. serratus*, the larger increase in carbon content at 200 °C shows that its carbohydrates were completely broken down at this temperature, without further improvement in carbon content as the temperature was increased.

Cellulose breaks down at the HTC temperatures used, accelerating at 220 °C, after which it shows a strong sensitivity to the change in processing conditions [36, 69]. Hence, the rapid increase in carbon content of CS-HC220 and CS-HC250 suggest that coconut shell is a cellulose

Table 3 Elemental and proximate analysis of adsorbents

Material	Elemental composition (%)						Proximate analysis (%)		
	C	H	N	O	H/C ratio	O/C ratio	Volatile matter	Fixed carbon	Ash
Raw FS	34.16	3.75	2.04	44.97	1.32	1.76	67.92	11.47	15.07
FS-HC200	52.20	5.82	2.76	24.06	1.34	0.62	63.28	18.66	15.17
FS-HC220	50.82	5.93	2.64	24.65	1.40	0.65	63.09	18.31	15.96
FS-HC250	52.67	7.44	2.64	19.20	1.70	0.49	60.15	19.24	18.05
Raw CS	48.57	6.79	0.92	37.58	1.68	1.03	72.19	17.90	6.15
CS-HC200	53.83	6.98	1.48	33.44	1.56	0.83	68.31	24.14	4.27
CS-HC220	59.34	7.06	0.83	28.16	1.43	0.63	63.51	28.69	4.63
CS-HC250	68.40	7.64	4.39	15.83	1.34	0.31	50.26	43.46	3.74
Raw Oak	46.61	6.86	0.73	42.20	1.77	1.21	81.90	9.56	3.60
Oak-HC200	52.95	6.28	1.35	32.70	1.42	0.82	73.51	16.96	6.73
Oak-HC220	53.44	6.28	1.00	31.11	1.41	0.78	67.39	22.00	8.17
Oak-HC250	56.02	6.43	1.42	17.42	1.38	0.42	51.04	28.13	18.72

Raw non-carbonised *Fucus serratus*, *Raw CS* non-carbonised coconut shell, *Raw Oak* non-carbonised oak. O = 100 − (C + H + N + Ash). Fixed carbon = 100 − (moisture + volatile matter + ash). Results of moisture content were not included

rich biomass [29]. The oak biomass is suggested to be a lignin rich biomass as a relatively considerable increase in the carbon content was obtained at 250 °C; since thermal decomposition of lignin has been found to occur at higher temperatures [33, 34].

As the HTC temperature was increased, there was a reduction in the oxygen content in all the hydrochars. This was caused by the release of oxygen to the liquid and gaseous fractions through the formation of species such as H_2O and CO_2 [12] via dehydration, decarboxylation and deoxygenation reactions. At high temperatures, the oxygen containing surface compounds were consumed more easily. As reported by Martinez-Mendoza et al. [70], this generates spaces in the structure through which fixed carbon is consumed allowing the widening of the pores. This is because intramolecular dehydration reactions [71] followed by decarboxylation reactions take place in the solid-to-solid conversion pathway [72].

Hydrogen content did not correlate with the expected volatile matter release as the temperature was increased. The loss in solid matter caused an overall increase in hydrogen content as the HTC temperature increased. The sharp increase in H content in FS-HC200 could be due to the considerable decomposition of the carbohydrates at 200 °C (as discussed in Sect. 3.1) cause by dehydration reactions. Apart from FS-HCs, H/C ratio decreased with an increase in HTC temperature, indicating that dehydration reaction occurred. There is a significant decrease in O/C ratio following carbonisation and reduced as the HTC temperature was increased. Lower H/C in the hydrochars indicate high degree of aromaticity, while lower O/C ratio represents low polarity and a decrease in the oxygen functional groups, making the hydrochars more hydrophobic [14, 73, 74] as the dehydration reactions removed the hydrophilic hydroxyl groups as the HTC temperature was increased. Also, the decrease in H/C and O/C atomic ratios at higher temperatures indicate an increase in the degree of condensation of the hydrochar materials [40]. The reduction of H/C and O/C atomic ratios as HTC temperature is increased have been reported for hydrochars derived from pure cellulose between 160 and 280 °C (i.e., H/C of 1.45–0.65, O/C of 0.82–0.23) [36], organic sludge carbonised between 180 and 240 °C (i.e., H/C of 2.08–1.58, O/C of 0.58–0.33) [75], and paper board mill sludge carbonised at temperatures ranging from 180 to 240 °C (i.e., H/C ratio of 1.52–1.09, O/C ratio of 0.60–0.36) [76]. The H/C and O/C ratios of Oak-HCs were within the range of values reported by Volpe et al. [36], and the H/C ratios of CS-HCs were similar to those reported by Oumabady et al. [76], whilst the O/C ratios of CS-HCs were within in the range of values reported by Volpe et al. [36].

3.6 Proximate analysis

As shown in Table 3, volatile matter of all the biomass reduced after carbonisation, and the content in the hydrochars further decreased as the HTC temperature was increased, producing more stable hydrochars less likely to contribute to any secondary pollution. HTC resulted in an increase in the fixed carbon content and the levels in the hydrochars increased with a rise in the HTC temperature. Martinez-Mendoza et al. [70] found that fixed carbon and volatile matter suggest the extent of carbonisation and relate to porosity development in the hydrochars, while an additional activation stage consumes fixed carbon from the char walls, causing them to widen. However, there was no activation process in this present study. During the HTC process, the volatile matter was converted into gases or more carbon rich products resulting in the formation of porosity of the hydrochars. Except for CS-HCs that saw a decrease in ash content following HTC and an increase in temperature, the ash content of FS-HCs and Oak-HCs increased with temperature. The very high increased in the ash content of the Oak-HC250 may be due to the precipitation of inorganic salts on the hydrochar during HTC at higher temperature [77], which correlated with the higher yield of the Oak-HC250 hydrochar (Table 1), caused by polymerisation reactions leading to continues reaction of the lignin intermediates to char [38]. High levels of ash content are undesirable as it blocks the micropores (< 10 nm), creating inactive sites [70], and reducing the mechanical properties of the adsorbents.

3.7 Functional groups

FTIR spectra of raw and produced hydrochars are presented in Figs. S13 to S15 (in the Supplementary Material). HTC resulted in significant changes to the surface functional groups of *F. serratus*, however, increasing HTC temperature did not have any further effect (shown in Fig. S13). This supports the explanation in Sect. 3.1 that the material is mainly comprised of alginates, laminarin, mannitol and fucoidan [42, 43], which was completely broken down at 200 °C. This is indicated by the broad and sharp band around 1047 cm^{-1} that is caused by glycosidic (C–O–C) bonds found in hemicellulose structures that decreased in intensity following the HTC process. One notable change caused by the HTC process is the broad reduction in the band at 3280 cm^{-1}, which corresponds to the O–H bonds in the materials. The raw *F. serratus* has bands at 1440 cm^{-1} and 1700 cm^{-1} that correspond to carboxylic acid groups [78]. However, the size of this band reduced during HTC. The band at 2970 cm^{-1} suggests the presence of stretching mode of aromatic C–C bonds, while the bands at 825 and 660 cm^{-1}, which

is hardly visible in the spectra, relate to the bending modes of aromatic rings. A change of these modes could suggest a change in aromatic character during HTC of FS. Feng et al. [79] attributed a similar absorbance at 828 cm^{-1} to the –CH bend in aromatics.

The coconut shell spectrum (shown in Fig. S14) shows the hydrolysis of hemicellulose represented by the band at 1040 cm^{-1}, which broaden in the raw sample and shorten in CS-HC200. The spectra of CS-HC200 and CS-HC220 are very comparable because of the stability of the cellulose at 200 and 220 °C. At 250 °C (i.e., CS-HC250), cellulose is broken down causing the band at 1040 cm^{-1} to disappear, leaving the glucose ring asymmetric valence vibration (C–O–C) shown by the band at 1106 cm^{-1} [80] and the bands at 1200, 1600, and 1700 cm^{-1}. The bands at 1200 and 1700 cm^{-1} could be attributed to the C=O carbonyl [36] due to the breakdown of lignin in the CS-H250 hydrochar at higher temperatures [33, 34]. The band at 1600 cm^{-1} decreased in intensity with an increase in temperature; this represents the aromatic groups. Increasing temperature to 250 °C decreased the intensity of the bands at 3280–3400 cm^{-1} in the hydrochars, which represent the O–H bonds found in alcohol that could provide sites for cationic pollutants to exchange onto. The reduction in O–H bonds suggests the occurrence of dehydration reactions during the carbonisation process [78].

The raw oak spectrum (Fig. S15) has a broad and sharp band around 1047 cm^{-1} that represents C–O–C (ether group) stretching vibrations caused by glycosidic bonds found in hemicellulose [80]. Once the oak was HTC treated, the hemicellulose was hydrolysed causing the band to become broader and smoother. According to Wang et al. [81], this band resembles the shape of cellulose which includes the band for ring vibration within its crystal structure. The band between 1000 and 1200 cm^{-1} represent C–O–C glycosidic bond vibration in cellulose, which remained almost the same between Oak-HC200 and Oak-HC220 but changed as the temperature was increased to 250 °C (i.e., in Oak-HC250). Liu et al. [82] reported that the region between 1000 and 1150 cm^{-1} corresponds to the strength vibration and the C–O–C glycosidic bond vibration, which is similar to bands between 1000 and 1200 cm^{-1} in Fig. S15. The band at 1106 cm^{-1} represents C–O–C ether group due to glucose ring asymmetric valence vibration [80], which means that some of structure of cellulose remained in the hydrochar although the intensity of the band at 1040 cm^{-1} representing C–O–C ether bond decreased suggesting that most of the cellulose has been hydrolysed. The bands found at 1700, 1600 and 1200 cm^{-1} were present in all the samples. The band at 1700 cm^{-1} represents C=O carboxylate groups [36], and 1600 cm^{-1} corresponds to aromatic C=C bond that make up a large amount of lignin's ring structure [80, 83].

Both groups were produced during the HTC process. Increasing temperature resulted in the production of glucose monomers from cellulose creating more C=O bonds [30]. The band at 1200 cm^{-1} corresponds to the C–O bond found in phenols and ethers, which remains in all the hydrochars. The broad band at 2900 cm^{-1} corresponds to aliphatic C-H bonds indicating that some fraction of the hydrochars remains unconverted to aromatic structures. At 250 °C, the Oak-HC250 band started to separate into two bands, corresponding to CH$_3$ and CH$_2$ of aliphatic chains, which can be linked to the breaking of lignocellulosic chains into aliphatic chains with increasing of temperature. The broad bands at 3280–3400 cm^{-1} show a large concentration of O–H bonds from water and alcohols present in the samples [81], which are not affected by the HTC temperature. The band at 1440 cm^{-1} corresponds to O–H carboxylic acid groups [81], which were found in all the oak samples.

4 Conclusions

This study has demonstrated that hydrochars prepared from *F. serratus* (FS-HCs), coconut shell (CS-HCs) and oak (Oak-HCs) through hydrothermal carbonisation (HTC) at different temperatures have different physicochemical adsorbent characteristics. HTC improved the surface area of the biomass with a further increased in the surface area of the produced hydrochars as the HTC temperature was increased to 250 °C (10.93–12.78 m^2/g for FS-HCs, 2.18–21.94 m^2/g for CS-HCs), with the exception of Oak-HCs that saw a decrease at higher HT temperatures (4.89–3.09 m^2/g). The decreased in the surface areas of Oak-HCs was as a result of the high abundance of microspheres which were caused by a solid-to-solid carbonisation of the non-dissolved components to form polymeric char. Increasing HTC temperature decreased volatile matter content in the hydrochars (53.28–60.15% for FS-HCS, 68.31–50.26% for CS-HCs, 73.51–51.04% for Oak-HCs) and increased fixed carbon (18.66–19.24% for FS-HCs, 24.14–43.46% for CS-HCs, 16.96–28.13% for Oak-HCs), resulting in more stable and porous hydrochars. Dehydration and decarboxylation reactions caused a decrease in H/C ratio (except for FS-HCs) and a reduction in O/C, which further decreased with increasing HTC temperature, indicating a high degree of aromaticity and low polarity, and a decreased in the amount of oxygenated surface functional groups. The study confirms that physicochemical adsorbent characteristics of hydrochars depend on the type of biomass feedstock and the HTC processing temperature utilised. However, a further study on adsorption of pollutants using these hydrochars is required to fully understand their sorption capacity, kinetics and isotherms.

Declarations

Conflict of interest The authors declare that they have no financial and non-financial conflict of interests.

References

1. Park K-H, Balathanigaimani MS, Shim W-G, Lee J-W, Moon H (2010) Adsorption characteristics of phenol on novel corn grain-based activated carbons. Microporous Mesoporous Mater 127:1–8

2. Kilic M, Apaydin-Varol E, Pütün AE (2011) Adsorptive removal of phenol from aqueous solutions on activated carbon prepared from tobacco residues: equilibrium, kinetics and thermodynamics. J Hazard Mater 189:397–403

3. Chiang C-H, Chen J, Lin J-H (2020) Preparation of pore-size tunable activated carbon derived from waste coffee grounds for high adsorption capacities of organic dyes. J Environ Chem Eng 8:103929

4. Ali I, Asim M, Khan TA (2012) Low cost adsorbents for the removal of organic pollutants from wastewater. J Environ Manage 113:170–183

5. Derbyshire F, Jagtoyen M, Andrews R, Rao A, Martin-Gullon I, Grulke EA (2001) Carbon materials in environmental applications. Chem Phys Carbon 27:1–66

6. Ahmaruzzaman M (2008) Adsorption of phenolic compounds on low-cost adsorbents: a review. Adv Colloid Interface Sci 143:48–67

7. Arena N, Lee J, Clift R (2016) Life cycle assessment of activated carbon production from coconut shells. J Clean Prod 125:68–77

8. Mihajlovic ML, Petrović J, Stojanovic M, Milojkovic J, Lopičić Z, Koprivica M, Lacnjevac C (2016) Hydrochars, perspective adsorbents of heavy metals: a review of the current state of studies. Zastita Materijala 57(3):488–495. https://doi.org/10.5937/zasmat1603488m

9. Sun K, Ro K, Guo M, Novak J, Mashayekhi H, Xing B (2011) Sorption of bisphenol A, 17α-ethinyl estradiol and phenanthrene on thermally and hydrothermally produced biochars. Bioresour Technol 102(10):5757–5763

10. Ahmed M, Rajapaksha A, Lim J, Zhang M, Bolan N, Mohan D, Ok Y (2014) Biochar as a sorbent for contaminant management in soil and water: a review. Chemosphere 99:19–33

11. Mohan D, Sarswat A, Ok Y, Pittman C (2014) Organic and inorganic contaminants removal from water with biochar, a renewable, low cost and sustainable adsorbents—a critical review. Bioresour Technol 160:191–202

12. Funke A, Ziegler F (2010) Hydrothermal carbonization of biomass: a summary and discussion of chemical mechanisms for process engineering. Biofuel Bioprod Biorefin -Biofpr 4(2):160–177

13. Libra J, Ro K, Kammann C, Funke A, Neubauer Y, Emmerich K (2011) Hydrothermal carbonization of biomass residues: a comparative review of the chemistry, processes and applications of wet and dry pyrolysis. Biofuels 2(1):71–106

14. Danso-Boateng E, Shama G, Wheatley AD, Martin SJ, Holdich RG (2015) Hydrothermal carbonisation of sewage sludge: effect of process conditions on product characteristics and methane production. Bioresour Technol 177:318–327

15. Titirici MM, Thomas A, Yu S-H, Müller J-O, Antonietti M (2007) A direct synthesis of mesoporous carbons with bicontinuous pore morphology from crude plant material by hydrothermal carbonization. Chem Mater 19(17):4205–4212. https://doi.org/10.1021/cm0707408

16. Román S, Ledesma B, Álvarez A, Herdes C (2018) Towards sustainable micro-pollutants' removal from wastewaters: caffeine solubility, self-diffusion and adsorption studies from aqueous solutions into hydrochars. Mol Phys 116(15–16):2129–2141. https://doi.org/10.1080/00268976.2018.1487597

17. Danso-Boateng E, Mohammed AS, Sander G, Wheatley AD, Nyktari E, Usen IC (2021) Production and characterisation of adsorbents synthesised by hydrothermal carbonisation of biomass wastes. SN Appl Sci 3:257

18. Goldfarb JL, Hubble AH, Ma Q, Volpe M, Giulia S, Andreottola G, Fiori L (2022) Valorisation of cow manure via hydrothermal carbonization for phosphorous recovery and adsorbents for water treatment. J Environ Manage 308:114561. https://doi.org/10.1016/j.jenvman.2022.114561

19. Islam MdA, Ahmed MJ, Khanday WA, Asif M, Hameed BH (2017) Mesoporous activated coconut shell-derived hydrochar prepared via hydrothermal carbonization-NaOH activation for methylene blue adsorption. J Environ Manage 203:237–244. https://doi.org/10.1016/j.jenvman.2017.07.029

20. Tu R, Sun Y, Wu Y, Fan X, Wang J, Shen X, He Z, Jiang E, Xu X (2019) Effect of surfactant on hydrothermal carbonization of coconut shell. Bioresour Technol 284:214–221. https://doi.org/10.1016/j.biortech.2019.03.120

21. Elaigwu SE, Greenway GM (2019) Characterization of energy-rich hydrochars from microwave-assisted hydrothermal carbonization of coconut shell. Waste Biomass Valoriz 10:1979–1987. https://doi.org/10.1007/s12649-018-0209-x

22. Saha N, Volpe M, Fiori L, Volpe R, Messineo A, Reza TM (2020) Cationic dye adsorption on hydrochars of winery and citrus juice industries residues: performance, mechanism, and

thermodynamics. Energies 13:4686. https://doi.org/10.3390/en13184686

23. Ahmady-Asbchin S, Andrès Y, Gérente C, Cloirec P (2008) Biosorption of Cu (II) from aqueous solution by *Fucus serratus*: surface characterization and sorption mechanisms. Bioresour Technol 99(14):6150–6155

24. Shahbandeh M (2021) Global coconut production 2000–2019. https://doi.org/https://www.statista.com/statistics/577497/world-coconut-production/. Accessed 3 August 2021

25. Magat SS (2003) Achieving coconut supply reliability through research-based crop nutrition management of coconut farms in the Philippines. CORD 19(01):34. https://doi.org/10.37833/cord.v19i01.363

26. Politi DV, Kopsidas ON, Batzias FA, Sidira DK (2013) Seaweed biomass for the removal of basic dyes from aqueous solutions. In: 21st European biomass conference and exhibition. 3–7 June 2013, Denmark, pp1055–1059

27. Arumugam N, Chelliapan S, Kamyab H, Thirugnana S, Othman N, Nasri NS (2018) Treatment of wastewater using seaweed: a review. Int J Environ Res Public Health 15(12):2851–2868. https://doi.org/10.3390/ijerph15122851

28. Liyanage CD, Pieris M (2015) A physico-chemical properties of coconut shell powder. Procedia Chem 16:222–228. https://doi.org/10.1016/j.proche.2015.12.045

29. Sangian HF, Widjaja A (2018) The effect of alkaline concentration on coconut husk crystallinity and the yield of sugars released. IOP Conf Ser: Mater Sci Eng 306:012046. https://doi.org/10.1088/1757-899X/306/1/012046

30. Floch AL, Jourdes M, Teissedre P-L (2015) Polysaccharides and lignin from oak wood used in cooperage: composition, interest, assays: a review. Carbohydr Res 417:94–102. https://doi.org/10.1016/j.carres.2015.07.003

31. (2008) ASTM Standard test methods for instrumental determination of carbon, hydrogen, and nitrogen in laboratory samples of coal, ASTM-D5373-08. ASTM International, Pennsylvania

32. (2010) ASTM Standard test methods for proximate analysis of coal and coke by macro thermogravimetric analysis, method D7582-10; ASTM International: Pennsylvania

33. Borrero-lópez AM, Masson E, Celzard A, Fierro V (2018) Modelling the reactions of cellulose, hemicellulose and lignin submitted to hydrothermal treatment. Ind Crops Prod 124:919–930. https://doi.org/10.1016/j.indcrop.2018.08.045

34. Mäkelä M, Volpe M, Volpe R, Fiori L, Dahl O (2018) Spatially resolved spectral determination of polysaccharides in hydrothermally carbonized biomass. Green Chem 20:1114–1120. https://doi.org/10.1039/C7GC03676K

35. Kang S, Li X, Fan J, Chang J (2012) Characterization of hydrochars produced by hydrothermal carbonization of lignin, cellulose, D-xylose, and wood meal. Ind Eng Chem Res 51(26):9023–9031

36. Volpe M, Messineo A, Mäkelä M, Barr MR, Volpe R, Corrado C, Fiori L (2020) Reactivity of cellulose during hydrothermal carbonization of lignocellulosic biomass. Fuel Process Technol 206:106456

37. Danso-Boateng E, Holdich RG, Shama G, Wheatley AD, Sohail M, Martin SJ (2013) Kinetics of faecal biomass hydrothermal carbonisation for hydrochar production. Appl Energy 111:351–357

38. Asghari FS, Yoshida H (2006) Acid-catalysed production of 5-hydroxymethyl furfural from D-fructose in subcritical water. Ind Eng Chem Res 45:2163–2173

39. Jain A, Balasubramanian R, Srinivasan MP (2016) Hydrothermal conversion of biomass waste to activated carbon with high porosity: a review. Chem Eng J 283:789–805. https://doi.org/10.1016/j.cej.2015.08.014

40. Sevilla M, Fuertes A (2009) The production of carbon materials by hydrothermal carbonization of cellulose. Carbon 47:2281–2289

41. Zhu X, Liu Y, Qian F, Zhou C, Zhang S, Chen J (2015) Role of hydrochar properties on the porosity of hydrochar-based porous carbon for their sustainable application. ACS Sustain Chem Eng 3:833–840. https://doi.org/10.1021/acssuschemeng.5b00153

42. Stiger-Pouvreau V, Bourgougnon N, Deslandes E (2016) Carbohydrates from seaweeds. In: Fleurence J, Levine I (eds) Seaweed in health and disease prevention. Elsevier, Amsterdam, pp 223–274. https://doi.org/10.1016/B978-0-12-802772-1.00008-7

43. Catarino MD, Silva AMS, Cardoso SM (2018) Phycochemical constituents and biological activities of Fucus spp. Mar Drugs 16(8):249. https://doi.org/10.3390/md16080249

44. Wang Y, Hu Y, Zhao X, Wang S, Xing G (2013) Comparisons of biochar properties from wood material and crop residues at different temperatures and residence times. Energy Fuels 27(10):5890–5899. https://doi.org/10.1021/ef400972z

45. Gurten I, Ozmak M, Yagmur E, Aktas Z (2012) Preparation and characterisation of activated carbon from waste tea using K_2CO_3. Biomass Bioenergy 37:73–81

46. Zhou J, Luo A, Zhao Y (2018) Preparation and characterisation of activated carbon from waste tea by physical activation using steam. J Air Waste Manage Assoc 68(12):1269–1277

47. Sivakumar SR, Arunkumar K (2009) Sodium, potassium and sulphate composition in some seaweeds occurring along the Coast of Gulf of Mannar, India. Asian J Plant Sci 8:500–504. https://doi.org/10.3923/ajps.2009.500.504

48. Brandt MJ, Johnson KM, Elphinston AJ, Ratnayaka DD (2017) Twort's water supply, 7th edn. Butterworth-Heinemann, Oxford. https://doi.org/10.1016/B978-0-08-100025-0.00007-7

49. Gacesa E, Squire A, Winterburn EJ (1983) The determination of the uronic acid composition of alginates by anion-exchange liquid chromatography. Carbohydr Res 118:1–8

50. Aydıncak K, Yumak T, Sınağ A, Esen B (2012) Synthesis and characterization of carbonaceous materials from saccharides (glucose and lactose) and two waste biomasses by hydrothermal carbonization. Ind Eng Chem Res 51:9145–9152

51. Liu Z, Zhang FS, Wu J (2010) Characterization and application of chars produced from pinewood pyrolysis and hydrothermal treatment. Fuel 89:510–514

52. Uzuner S, Cekmecelioglu D (2014) Hydrolysis of hazelnut shells as a carbon source for bioprocessing applications and fermentation. Int J Food Eng 10(4):799–808. https://doi.org/10.1515/ijfe-2014-0158

53. Domingos I, Ferreira J, Cruz-Lopes LP, Esteves B (2022) Liquefaction and chemical composition of walnut shells. Open Agric 7:249–256. https://doi.org/10.1515/opag-2022-0072

54. Kovačić D, Kralik D, Rupčić S, Jovičić D, Spajić R, Tišma M (2017) Soybean straw, corn stover and sunflower stalk as possible substrates for biogas production in Croatia: a review. Chem Biochem Eng Q 31(3):187–198

55. Xue Y, Gao B, Yao Y, Inyang M, Zhang M, Zimmerman AR, Ro KS (2012) Hydrogen peroxide modification enhances the ability of biochar (hydrochar) produced from hydrothermal carbonization of peanut hull to remove aqueous heavy metals: batch and column tests. Chem Eng J 200:673–680

56. Sevilla M, Maciá-Agulló JA, Fuertes AB (2011) Hydrothermal carbonization of biomass as a route for the sequestration of CO_2: chemical and structural properties of the carbonized products. Biomass Bioenergy 35:3152–3159

57. Bharthare P, Shrivastava P, Singh P, Ttiwari A (2014) Peanut shell as renewable energy source and their utility in production of ethanol. Int J Adv Res (IJOAR) 2(4):ISSN2320–9178

58. Roman S, Valente Nabais J, Ledesma B, González J, Laginhas C, Titirici M (2013) Production of low-cost adsorbents with tunable surface chemistry by conjunction of hydrothermal

carbonization and activation processes. Microporous Mesoporous Mater 165:127–133

59. Rodríguez G, Lama A, Rodríguez R, Jiménez Ana, Guillén R, Fernández-Bolaños J (2008) Olive stone an attractive source of bioactive and valuable compounds. Bioresour Technol 99(13):5261–5269. https://doi.org/10.1016/j.biortech.2007.11.027

60. Sun JX, Xu F, Sun XF, Xiao B, Sun RC (2005) Physico-chemical and thermal characterization of cellulose from barley straw. Polym Degrad Stabil 88(3):521–531

61. Jonar N, Ahmed I, Dufresne A (2012) Extraction, preparation and characterization of cellulose fibres and nanocrystals from rice husk. Ind Crops Prod 37(1):93–99. https://doi.org/10.1016/j.indcrop.2011.12.016

62. Veltri F, Alessandro F, Scarcello A, Beneduci A, Polanco MA, Perez DC et al (2020) Porous carbon materials obtained by the hydrothermal carbonization of orange juice. Nanomaterials 10:655. https://doi.org/10.3390/nano10040655

63. Sevilla M, Fuertes AB (2009) Chemical and structural properties of carbonaceous products obtained by hydrothermal carbonization of saccharides. Chem Eur J 15:4195–4203

64. Malvern Panalytical (2019) Water treatment and the role of zeta potential in water treatment process control. AZoNano. https://doi.org/https://www.azonano.com/article.aspx?ArticleID=1237. Accessed 25 Mar 2022

65. Malvern Instruments Limited (2015) Zeta potential—an introduction in 30 minutes. Technical note. Spectris plc. https://doi.org/https://www.research.colostate.edu/wp-content/uploads/2018/11/ZetaPotential-Introduction-in-30min-Malvern.pdf. Accessed 25 Mar 2022

66. López-Maldonado EA, Oropeza-Guzman MT, Jurado-Baizaval JL, Ochoa-Terán A (2014) Coagulation–flocculation mechanisms in wastewater treatment plants through zeta potential measurements. J Hazard Mater 279:1–10. https://doi.org/10.1016/j.jhazmat.2014.06.025

67. Chung JW, Edewi OC, Foppen JW, Gerner G, Krebs R, Lens PNL (2017) Removal of escherichia coli by intermittent operationof saturated sand columns supplemented withhydrochar derived from sewage sludge. Appl Sci 7:839. https://doi.org/10.3390/app7080839

68. Wang X, Hao W, Zhang P, Szego AE, Svensson G, Hedin N (2021) Macroscopic rods from self-assembled colloidal particles of hydrothermally carbonized glucose and their use as templates for SiC and Cu_3Si. J Colloid Interface Sci 602:480–489. https://doi.org/10.1016/j.jcis.2021.06.016

69. Saha N, Saba A, Reza MT (2019) Effect of hydrothermal carbonization temperature on pH, dissociation constants, and acidic functional groups on hydrochar from cellulose and wood. J Anal Appl Pyrolysis 137:138–145

70. Martínez-Mendoza KL, Barraza-Burgos JM, Marriaga-Cabrales N, Machuca-Martinez F, Barajas M, Romero M (2020) Production and characterization of activated carbon from coal for gold adsorption in cyanide solutions. Ingeniería e Investigación 40(1):34–44. https://doi.org/10.15446/ing.investig.v40n1.80126

71. Falco C, Baccile N, Titirici M-M (2011) Morphological and structural differences between glucose, cellulose and lignocellulosic biomass derived hydrothermal carbons. Green Chem 13:3273–3281. https://doi.org/10.1039/c1gc15742f

72. Paksung N, Pfersich J, Arauzo PJ, Jung D, Kruse A (2020) Structural effects of cellulose on hydrolysis and carbonization behavior during hydrothermal treatment. ACS Omega 5(21):12210–12223. https://doi.org/10.1021/acsomega.0c00737

73. Wani I, Sharma A, Kushvaha V, Madhushri P, Peng L (2020) Effect of pH, volatile content, and pyrolysis conditions on surface area and O/C and H/C ratios of biochar: towards understanding performance of biochar using simplified approach. J Hazard Toxic Radiact Waste 24(4):04020048

74. Liu Z, Quek A, Hoekman SK, Balasubramanian R (2013) Production of solid biochar fuel from waste biomass by hydrothermal carbonization. Fuel 103:943–949

75. Wang W, Chen W-H, Jang M-F (2020) Characterization of hydrochar produced by hydrothermal carbonization of organic sludge. Future Cities Environ 6(1):13. https://doi.org/10.5334/fce.102

76. Oumabady S, Sebastian PS, Kamaludeen SPB, Ramasamy M, Kalaiselvi P, Parameswari E (2020) Preparation and characterization of optimized hydrochar from paper board mill sludge. Sci Rep 10:773. https://doi.org/10.1038/s41598-019-57163-7

77. Zhang JH, Lin QM, Zhao XR (2014) The hydrochar characters of municipal sewage sludge under different hydrothermal temperatures and durations. J Integr Agric 13(3):471–482. https://doi.org/10.1016/S2095-3119(13)60702-9

78. Kruse A, Zevaco T (2018) Properties of hydrochar as function of feedstock, reaction conditions and post-treatment. Energies 11(3):674

79. Feng S, Yuan Z, Leitch M, Shui H, Xu CC (2016) Effects of bark extraction before liquefaction and liquid oil fractionation after liquefaction on bark-based phenol formaldehyde resoles. Ind Crops Prod 84:330–336. https://doi.org/10.1016/j.indcrop.2016.02.022

80. Salim MdR, Asik J, Sarjadi MS (2021) Chemical functional groups of extractives, cellulose and lignin extracted from native *Leucaena leucocephala* bark. Wood Sci Technol 55:295–313. https://doi.org/10.1007/s00226-020-01258-2

81. Wang S, Lin H, Zhang L, Dai G, Zhao Y, Wang X, Ru B (2016) Structural characterization and pyrolysis behavior of cellulose and hemicellulose isolated from softwood pinus armandii franch. Energy Fuels 30(7):5721–5728

82. Liu L, Cao J, Huang J, Cai Y, Yao J (2010) Extraction of pectins with different degrees of esterification from Mulberry branch bark. Bioresour Technol 101(9):3268–3273. https://doi.org/10.1016/j.biortech.2009.12.062

83. Tian M, Wen J, MacDonald D, Asmussen RM, Chen A (2010) A novel approach for lignin modification and degradation. Electrochem Commun 12(4):527–530. https://doi.org/10.1016/j.elecom.2010.01.035